Modelling tree ring cellulose $\delta^{18}O$ variations of two temperature-sensitive tree species from North and South America

Authors:

Aliénor Lavergne[1], Fabio Gennaretti[1], Camille Risi[2], Valérie Daux[3], Etienne Boucher[4], Martine M. Savard[5], Maud Naulier[6], Ricardo Villalba[7], Christian Bégin[5] and Joël Guiot[1]

[1] Aix Marseille Université, CNRS, IRD, Collège de France, CEREGE, ECCOREV, Aix-en-Provence, France

[2] Laboratoirede Météorologie Dynamique, IPSL, UPMC, CNRS, Paris, France

[3] Laboratoire des Sciences du Climat et de l'Environnement, CEA-CNRS-UVSQ, 91191 Gif-sur-Yvette, France

[4] Department of Geography and GEOTOP, Université du Québec à Montréal, Montréal, Canada

[5] Geological Survey of Canada, Natural Resources Canada, 490 rue de la Couronne, QC, G1K9A9, Canada

[6] Institut de Radioprotection et de Sureté Nucléaire (IRSN), PRP-ENV, SERIS/LRTE, Saint-Paul-lez-Durance, France

[7] Instituto Argentino de Nivología, Glaciología y Ciencias Ambientales, IANIGLA-CONICET, Mendoza, Argentina

Corresponding authors: Aliénor Lavergne (alienor.lavergne@gmail.com) and Fabio Gennaretti (gennaretti@cerege.fr)

Tel : +33 (0) 4 42 97 15 32

Centre Européen de Recherche et d'Enseignement en Géosciences

Technopôle de l'Arbois-Méditerranée

13545 Aix-en-Provence, FRANCE

ABSTRACT

Oxygen isotopes in tree rings ($\delta^{18}O_{TR}$) are widely used to reconstruct past climates. However, the complexity of climatic and biological processes controlling isotopic fractionation is not yet fully understood. Here, we use the MAIDENiso model to decipher the variability of $\delta^{18}O_{TR}$ of two temperature-sensitive species of relevant paleoclimatological interest (*Picea mariana* and *Nothofagus pumilio*) and growing at cold high-latitudes in North and South America. In this first modelling study on $\delta^{18}O_{TR}$ values in both northeastern Canada (53.86°N) and western Argentina (41.10°S), we specifically aim at: 1) evaluating the predictive skill of MAIDENiso to simulate $\delta^{18}O_{TR}$ values, 2) identifying the physical processes controlling $\delta^{18}O_{TR}$ by mechanistic modelling and, 3) defining the origin of the temperature signal recorded in the two species. Although the linear regression models used here to predict daily $\delta^{18}O$ of precipitation ($\delta^{18}O_P$) may need to be improved in the future, the resulting daily $\delta^{18}O_P$ values adequately reproduce observed (from weather stations) and simulated (by global circulation model) $\delta^{18}O_P$ series. The $\delta^{18}O_{TR}$ values of the two species are correctly simulated using the $\delta^{18}O_P$ estimation as MAIDENiso input, although some offset in mean $\delta^{18}O_{TR}$ levels is observed for the South American site. For both species, the variability of $\delta^{18}O_{TR}$ series is primarily linked to the effect of temperature on isotopic enrichment of the leaf water. We show that MAIDENiso is a powerful tool for investigating isotopic fractionation processes but that the lack of a denser isotope-enabled monitoring network recording oxygen fractionation in the soil-vegetation-atmosphere compartments limits our capacity to decipher the processes at play. This study proves that the eco-physiological modelling of $\delta^{18}O_{TR}$ values is necessary to interpret the recorded climate signal more reliably.

Keywords: MAIDENiso model, $\delta^{18}O$, tree ring, *Nothofagus pumilio*, *Picea mariana*

1. INTRODUCTION

Oxygen isotopes in tree rings ($\delta^{18}O_{TR}$) are increasingly used as indicators of past climatic changes in temperate areas (Cernusak and English, 2015; Hartl-Meier et al., 2014; Saurer et al., 2008). They have been widely used to reconstruct past atmospheric conditions such as air temperature (Naulier et al., 2015), drought (Labuhn et al., 2016), precipitation amount (Rinne et al., 2013), isotopic composition of precipitation (Danis et al., 2006), relative air humidity (Wernicke et al., 2015), cloud cover (Shi et al., 2012), and even atmospheric circulation patterns (Brienen et al., 2012). This diversity of climatic targets possibly reconstructed based on oxygen isotopes hints at the challenge of understanding the complexity of the climatic and biological processes that control isotopic fractionation of oxygen in trees (Treydte et al., 2014). Uncertainties arise because different poorly measured factors influence $\delta^{18}O_{TR}$ values. Isotopic signals in tree rings cellulose are strongly influenced by isotopic signature of soil water taken up by the roots and by evaporative and physiological processes occurring at the leaf level and during downstream metabolism (Barbour et al., 2005; Gessler et al., 2014). Thus, a comprehensive approach that embraces existing mechanistic understanding of the fractionation processes involved is required.

Few isotopic process-based models have been developed to investigate the mechanistic rules governing the $\delta^{18}O_{TR}$ variations (Guiot et al., 2014): the Péclet-modified Craig-Gordon model (Kahmen et al., 2011) and the Roden's model (Roden et al., 2000) are able to estimate, at a daily time step, the $\delta^{18}O$ values of soil and xylem waters, and the isotopic fractionation occurring in the leaves due to evapotranspiration. Versions of these models are integrated in more complete forest ecophysiological models simulating the ensemble of forest water and carbon fluxes: (1) MAIDEN (Modeling and Analysis In DENdroecology) (Gea-Izquierdo et al., 2015; Misson, 2004), which contains the isotopic module MAIDENiso (Danis et al., 2012) and (2) MUSICA (Ogée et al., 2003, 2009). Both are accounting for important post-photosynthetic factors and are able to link photosynthesis and carbohydrate allocation to stem growth.

In this paper, we use the MAIDENiso model to decipher the $\delta^{18}O_{TR}$ variability in American temperature-sensitive species (*Picea mariana* in northeastern Canada and *Nothofagus pumilio* in western Argentina). The selected sites are of special interest for paleoclimatology given that their

86 $\delta^{18}O_{TR}$ chronologies carry strong temperature signals. A summer temperature reconstruction was

87 already developed at the North American site (Gennaretti et al., 2017b; Naulier et al., 2015) and a

88 calibration study conducted at the South American one highlighted the strong potential of $\delta^{18}O_{TR}$

89 values to reflect variations in summer-autumn temperatures over a large region south of 38°S

90 (Lavergne et al., 2016). However, up to now, the climate-$\delta^{18}O_{TR}$ relationships were analysed

91 using a black box approach based on linear models. Here, we specifically aim at: 1) evaluating

92 the predictive skill of MAIDENiso to simulate $\delta^{18}O_{TR}$ values, 2) identifying the physical

93 processes controlling $\delta^{18}O_{TR}$ by mechanistic modelling and, 3) defining the origin of the

94 temperature signal recorded in the two species.

95

96 **2.   DATA AND METHODS**

97 **2.1. Sampling sites and tree-ring data**

98 Two high-latitude American native species were studied here: 1) *Picea mariana* (Mill. B.S.P.;

99 black spruce), which is a conifer widely distributed over the American boreal forest (Viereck and

100 Johnston, 1990); and 2) *Nothofagus pumilio* (Poepp. et Endl. Krasser; lenga), which is an

101 angiosperm deciduous species dominating the high-elevation forests along the Patagonian Andes

102 from 35°S to 55°S (Donoso, 1981; Schlatter, 1994). We selected two sites of *P. mariana* in the

103 centre of the Quebec-Labrador Peninsula in northeastern Canada (L01 and L20; from 53°51'N-

104 72°24'W to 54°33'N-71°14'W, ~480 m elevation; see Gennaretti et al. (2014) and Naulier et al.

105 (2014) for details) and three sites of *N. pumilio* in northern Patagonia, western Argentina (NUB,

106 ALM and CHA; from 41°09′S-71°48′W to 41°15′S-71°17′W, 1270-1610 m elevation; see

107 Lavergne et al. (2016, 2017) for details). Climate in northeastern Canada is mostly continental

108 and subarctic with short, mild and wet summers and long, cold and dry winter. Total annual

109 precipitation averages 825 mm with up to 46% falling during the growing season in summer

110 (June to September) (Naulier et al., 2014). In western Argentina, precipitation is largely

111 concentrated from late fall to early spring (May-November) followed by a drier and mild period

112 during summer and early fall (December-April) (López Bernal et al., 2012).

113

114 Four trees per site were collected for both species. The selection of the samples and analytical

115 procedure for $\delta^{18}O_{TR}$ measurements were described in Lavergne et al. (2016) and Naulier et al.

116   (2014). The developed $\delta^{18}O_{TR}$ chronologies covered the 1950-2005 and 1952-2011 periods at the

117   northeastern Canadian and western Argentinian sites, respectively. The chronologies that were

118   built for each species were significantly correlated between stands (Figure 1). This supported the

119   construction of a combined isotope chronology for both the northeastern Canada and western

120   Argentina sites.

121

122   **2.2. Modelling oxygen isotopes in tree ring cellulose with MAIDENiso**

123   MAIDENiso is a process-based model that can simulate in parallel phenological and

124   meteorological controls on photosynthetic activity and carbon allocation (Danis et al., 2012). It

125   explicitly allocates carbohydrates to different carbon pools (leaves, stem, storage and roots) on a

126   daily basis using phenological stage-dependent rules (see Gennaretti et al. (2017b) for details on

127   the construction of the main MAIDEN model). It also simulates the fractionation of carbon and

128   oxygen isotopes during growth processes. In particular, it estimates at a daily time step $\delta^{18}O$

129   values of soil water and xylem water, the isotopic fractionation occurring in the leaves due to

130   evapotranspiration and the biochemical fractionation during cellulose formation. It uses as input

131   daily maximum and minimum temperature (°C), precipitation (cm/day), atmospheric CO_2

132   concentration (ppm) and $\delta^{18}O$ values of precipitation ($\delta^{18}O_P$ in ‰).

133

134   In this study, the calculation of the daily $\delta^{18}O_{TR}$ in tree ring cellulose (‰) is based on the (Danis

135   et al., 2012)'s formulation of the Craig-Gordon model (Craig and Gordon, 1965):

136            $\delta^{18}O_{TR} = (1-f_o)\cdot[\varepsilon^* + \varepsilon_k\cdot(1-h_{air}) + h_{air}\cdot\delta^{18}O_V + (1-h_{air})\cdot\delta^{18}O_{XW}] + f_o\cdot\delta^{18}O_{XW} + \varepsilon_0$ (1)

137   This equation summarizes how $\delta^{18}O_{TR}$ is determined by:

138   (i)   the $\delta^{18}O$ of the source (xylem) water ($\delta^{18}O_{XW}$), which is computed by averaging the

139               $\delta^{18}O_{SW}$ values of the different soil layers weighted by the volume of water taken up by

140   the roots in each layer. The isotopic effects of water mixing and soil evaporation on

141   the $\delta^{18}O_{SW}$ values of the different soil layers are computed by a mass and isotopic

142   balance (Danis et al., 2012). It is worth noting that no fractionation occurs during

143   water uptake by roots (Wershaw et al., 1966), neither during the transport of water

144   from the roots to the leaves.

145   (ii)   the ^{18}O enrichment of the leaf water due to transpiration is described by

146               $(\varepsilon^* + \varepsilon_k\cdot(1-h_{air}) + h_{air}\cdot\delta^{18}O_V + (1-h_{air})\cdot\delta^{18}O_{XW})$ after Craig and Gordon (1965), where:

147   a. ε^* is the equilibrium fractionation due to the change of phase from liquid water to vapour at the leaf temperature (fixed at 21.4°C, the temperature threshold for maximum carbon assimilation, ε^* is 9.65‰ (Helliker and Richter, 2008)),

150   b. ε_k is the kinetic fractionation due to the diffusion of vapour into unsaturated air through the stomata and the leaf boundary layer,

152   c. h_{air} is the relative humidity of the evaporating air mass estimated from daily air temperature (T_{air}; °C; mean of the maximum and minimum air temperatures), and the dew point temperature (T_r; °C) (Running et al., 1987),

155   d. $\delta^{18}O_V$ is the atmospheric water vapour calculated assuming a precipitation-vapour isotopic equilibrium (see below);

157   (iii)   the biochemical fractionations (ε_0) due to oxygen exchange between carbonyl groups (C = O) in the organic molecules and water (DeNiro and Epstein, 1979; Farquhar et al., 1998).

160   (iv)   the dampening factor f_o reflecting the exchange of the oxygen atoms between sucrose and xylem water during cellulose synthesis in the xylem cells of tree rings.

162 As previously evoked (i), $\delta^{18}O_{XW}$ of Eq. 1 depends on $\delta^{18}O_{SW}$ and thus on $\delta^{18}O_P$ values. However, long continuous time series of $\delta^{18}O_P$ are not available in the studied area. Here, we tested the impact of using two different methods for deriving $\delta^{18}O_P$ time series.

165 First, a linear model was used to estimate the daily values of $\delta^{18}O_P$ and subsequently $\delta^{18}O_V$ based on the primary drivers of their temporal variability (Dansgaard, 1964; Horita and Wesolowski, 1994), that are air temperature (T_{air}; °C) and precipitation at the corresponding site (P; mm):

$$\delta^{18}O_P = a \cdot T_{air} + b \cdot P + c \tag{2}$$

$$\delta^{18}O_V = \delta^{18}O_P - \varepsilon^*_{Tair} \tag{3}$$

170 with ε^*_{Tair} the fractionation due to the change of phase from liquid water to vapour at the mean air temperature. The coefficients *a* and *b* were allowed to vary over a plausible range (or prior range) in the calibration process together with other MAIDENiso parameters, while coefficient *c* was fixed to a likely value (see Table 1 and section 2.4). This estimated set of data is referred in the following as the estimated $\delta^{18}O_P$ dataset.

175 Second, we run the model with the series of the daily $\delta^{18}O_P$ derived from two general circulation models (GCM) with different spatial resolutions and enough available data at our site locations:

177 1) the Melbourne University model (MUGCM; Noone and Simmonds, 2002) forced by varying

178 sea surface temperature (SST) from the HadISST data set for the 1950-2003 period (2°×2°

179 resolution; hereafter referred as MUGCM $\delta^{18}O_P$ dataset), and 2) the Laboratoire de Météorologie

180 Dynamique Zoom model (LMDZ5A; Hourdin et al. (2013); Risi et al. (2010)) with the horizontal

181 winds guided by those of the National Centers for Environmental Protection - 20th Century

182 Reanalysis (NCEP20) for the 1950-2008 period (Compo et al., 2011) (2.5°×3.75° resolution;

183 hereafter referred as LMDZ-NCEP20 $\delta^{18}O_P$ dataset).

184

185 The final $\delta^{18}O_{TR}$ time series are the annual average of the $\delta^{18}O_{TR}$ daily values (Eq. 1) weighted by

186 the daily simulated stand Gross Primary Production (GPP), assuming a proportional allocation of

187 carbon to the trunk. For the northeastern Canadian sites, the GPP simulated by MAIDENiso was

188 optimized using observations from an eddy covariance station (see Gennaretti et al. (2017a)).

189 Unfortunately, such observations were not available for *N. pumilio*, and therefore the

190 parameterization obtained for the GPP of *P. mariana* was also used for the western Argentinian

191 sites but constraining the simulations with phenological observations extracted from the

192 literature. For example, to respect the annual cycle of the leaf area index (LAI) for *N. pumilio*

193 (Magnin et al., 2014; Rusch, 1993), we used in MAIDENiso a seasonal LAI annual cycle with a

194 development of leaves (LAI increase) between October and November, a maximum LAI (set at 5

195 leaf area/ground area) from November to April, a decreasing LAI (leaf fall) between April and

196 May, and finally a leafless period (null LAI) from June to September (Magnin et al., 2014;

197 Rusch, 1993). Furthermore, based on the finding that $\delta^{18}O_{TR}$ annual time series were more

198 correlated to climate variables of specific months of the growing season (Lavergne et al., 2016),

199 we also computed $\delta^{18}O_{TR}$ annual values by weighting the $\delta^{18}O_{TR}$ daily values (Eq. 1) with

200 synthetic GPP time series maximizing the correspondence between observations and simulations.

201

2.3. Meteorological and atmospheric CO_2 data

203 At the western Argentinian sites, we did not have long daily records of observed climate data.

204 Therefore, daily minimum–maximum temperature and precipitation data were derived from the

205 20th Century Reanalysis V2c (2°×2° resolution; Compo et al., 2011), which is one of the few

206 reanalysis products covering entirely the 20th century. The temperature daily time series of the

207 reanalysis were corrected in order to respect the monthly mean values detected at Bariloche, the

208 nearest meteorological station from our sampling sites (~48 km from the sites, 41°12′ S–71°12′
209 W, 840 m asl; Servicio Meteorológico Nacional, Argentina). The resulting maximum and
210 minimum temperature series, covering the 1952-2011 period, fit well with the daily local
211 temperature data from La Almohadilla (ALM) site (41°11'S, 71°47'W, 1410 m asl; data
212 measured by dataloggers and provided by IANIGLA) available over the 2002-2012 period (r =
213 0.74, p < 0.001; Figure SM1). For the northeastern Canadian sites, climate data were obtained
214 from the gridded interpolated Canadian database of daily minimum–maximum temperature and
215 precipitation covering the 1950-2005 studied period (0.08°×0.08° resolution; Hutchinson et al.,
216 2009). In addition to these data we also used modelled daily data from the GCMs described
217 above for both the western Argentinian and northeastern Canadian sites (see Table 2 with the
218 input data used for each tested configuration).

219

220 Data on the atmospheric CO_2 concentration were derived from the Mauna Loa station over the
221 1958-2012 period (Keeling et al., 1976). For the years 1950-1957, we extrapolated atmospheric
222 CO_2 data using the trend and seasonal cycle as displayed in the observations over the subsequent
223 10-years period (1958-1967).

224
225 ## 2.4. Estimation of parameters influencing $\delta^{18}O_{TR}$

226 We used a Bayesian method for the simultaneous calibration of the various MAIDENiso
227 parameters specific to the study species and site. A set of 50 plausible blocks of parameters
228 (posterior values) was selected according to the method described in Gennaretti et al. (2017a)
229 using Markov Chain Monte Carlo (MCMC) sampling (Table 1). The following prior plausible
230 ranges were considered:
231 1) the prior ranges of the *a* and *b* coefficients in the equation of the daily $\delta^{18}O_P$ (Eq. 2) were
232 selected in order to get $\delta^{18}O_P$ values for each site consistent with the measured monthly local
233 values from the nearest stations of the Global Network of Isotopes in Precipitation (GNIP), and
234 with the simulated daily values from the LMDZ-NCEP20 model and from the MUGCM model
235 (see Table 1),
236 2) the range for the biochemical fractionation factor ε_0 was chosen between 24‰ and 30‰
237 (+27±3‰ after DeNiro and Epstein (1981), Sternberg (1989) and Yakir and DeNiro (1990)),

238   3) the range for the kinetic fractionation ε_k, which has been set to 26.5‰ in Farquhar et al. (1989)

239   but that can vary over larger ranges (Buhay et al., 1996), was taken between 10‰ and 30‰ here,

240   4) the range for the dampening factor f_o was allowed to vary between 0.3 and 0.5 following

241   Saurer et al. (1997).

242

243   We tested the sensitivity of the MAIDENiso model to the calibrated parameters by modifying

244   them within their respective prior calibration range. To control the robustness of the calibrated

245   parameters, we performed the calibration of these parameters over two equal length intervals

246   (1950-1977 and 1978-2005 for *P. mariana*; 1952-1981 and 1982-2011 for *N. pumilio*) keeping

247   the second half for independent validation of the parameters estimates. Once the model was

248   calibrated for the two species, the MAIDENiso's performance to simulate *P. mariana* and *N.*

249   *pumilio* $\delta^{18}O_{TR}$ interannual data was evaluated using the correlation coefficients (r) and the root

250   mean square errors (RMSE) between observed and simulated values. This is a standard approach

251   to evaluate how well a mechanistic model is simulating $\delta^{18}O_{TR}$ variations (e.g., Danis et al., 2012;

252   Lorrey et al., 2016).

253

254   **2.5. Disentangling leaf-level fractionation processes and source water influences on**

255   **$\delta^{18}O_{TR}$ signature**

256   To define the relative contributions to the $\delta^{18}O_{TR}$ signature of the isotopic signal of the source

257   water (xylem water) and of the fractionation processes due to transpiration taking place in the

258   leaves, we designed two experimental simulations with MAIDENiso based on Eq. 1:

259   1) to quantify the influence of the variability of the isotopic composition of the xylem water

260   on $\delta^{18}O_{TR}$, we compared the reference simulations to those where the relative humidity

261   (h_{air}) and the isotopic composition of atmospheric vapour ($\delta^{18}O_V$) were assumed to be

262   constant. The constant values for h_{air} and $\delta^{18}O_V$ were defined as the averages of the

263   respective MAIDENiso outputs (h_{air} = 0.62 and 0.9, and, $\delta^{18}O_V$ = -26.28‰ and -17.34‰,

264   respectively for northeastern Canada and western Argentina; the XW source experiment

265   simulation hereafter),

266   2) to quantify the influence of the isotopic enrichment of the leaf water due to transpiration

267   on $\delta^{18}O_{TR}$, we compared the reference simulations to those where the $\delta^{18}O_{XW}$ series were

268   assumed to be constant. The constant value for $\delta^{18}O_{XW}$ was estimated as the average of

269   the $\delta^{18}O_{XW}$ MAIDENiso outputs ($\delta^{18}O_{XW}$ = -13.81‰ and -7.03‰, respectively for

270   northeastern Canada and western Argentina; the Leaf water enrichment driven experiment

271   simulation hereafter).

272   Comparison between the experimental and reference simulations (i.e. using the optimal values of

273   the parameters) was achieved through the calculation of the coefficient of determination (R^2).

274

275   **3. RESULTS**

276   **3.1. Estimated versus modelled and observed $\delta^{18}O_P$ values**

277   The modelled $\delta^{18}O_P$ series from the GCM models are similar to the GNIP datasets, with mean

278   values ranging from -12‰ to -8‰ over June-September in northeastern Canada (Figure SM2A)

279   and from -7‰ to -3‰ over December-April at the western Argentinian sites (Figure SM2B). In

280   general, $\delta^{18}O_P$ series from LMDZ-NCEP20 model in western Argentina are slightly displaced

281   toward higher values (+1‰) in comparison with the GNIP and MUGCM data. The estimated

282    $\delta^{18}O_P$ values based on plausible values of coefficients *a* and *b* agree well with those of the models

283   and observations in northeastern Canada. For the western Argentinian sites, they are 2-3‰ lower

284   from April to October, i.e. late spring-early autumn (Figure SM2).

285

286   **3.2. Sensitivity of the model to the calibrated parameters**

287   Most of the calibrated parameters have an influence on the correlations between observed and

288   simulated $\delta^{18}O_{TR}$ series and/or on the mean levels of the simulated series (Figure 2). The

289   temperature and precipitation dependences of $\delta^{18}O_P$ values (respectively *a* and *b* coefficients)

290   have the strongest influence on correlations. Increasing *a* and *b* values increase the mean $\delta^{18}O_{TR}$

291   levels, more strongly in western Argentina than in northeastern Canada (Figure 2). Changes in

292   the dampening factor (f_o) and in the biochemical fractionation (ε_0) have almost no effect on

293   correlation, but their increase induces significant decrease of the mean levels of $\delta^{18}O_{TR}$ series.

294   Finally, increasing the kinetic fractionation (ε_k) leads to lower correlations and to higher mean

295   levels of $\delta^{18}O_{TR}$ (Figure 2).

296

297   **3.3. MAIDENiso performance in reproducing observed $\delta^{18}O_{TR}$ series**

298   Split-period verifications of the calibrated relationships for *P. mariana* and *N. pumilio* when

299   using estimated $\delta^{18}O_P$ series from Eq. 2 indicate that the calibration over either the first half or the

300 second half periods provide similar posterior densities of the calibrated parameters than the ones
301 obtained when calibrating over the whole periods (Figure SM3). One exception is observed in the
302 calibration of coefficient *a* in northeastern Canada over the two half periods, where the posterior
303 densities of *a* are different from the one obtained by calibrating over the entire period. Over the
304 entire periods, observed and simulated $\delta^{18}O_{TR}$ series are significantly correlated in northeastern
305 Canada (r = 0.56, p < 0.01 and RMSE = 0.67; Figure 3A) and in western Argentina (r = 0.48, p <
306 0.01 and RMSE = 0.63; Figure 3C). The correlation between observed and simulated $\delta^{18}O_{TR}$
307 series are slightly improved when we used synthetic daily GPP (r = 0.62 and r = 0.52, p < 0.01,
308 respectively for northeastern Canada and western Argentina; Figure 3B and 3D). It is worth
309 noting that the mean levels of the simulated $\delta^{18}O_{TR}$ series for the Argentinian sites are lower than
310 those of the observations (offset of around -2.5‰; Figure SM4). The series were therefore
311 corrected to respect the mean values detected in the observations (Figure 3C and 3D). In contrast,
312 the correlations between observation and simulation considerably decrease when we used
313 modelled $\delta^{18}O_P$ from MUGCM models or LMDZ-NCEP20 reanalysis data. They only reach
314 r = 0.13 (p > 0.05) to 0.23 (p < 0.05) in northeastern Canada and r = 0.23 to 0.26 (p < 0.05) in
315 western Argentina, respectively (Figure 4).

316

317 **3.4. Influence of source water and leaf water isotopic enrichment to the $\delta^{18}O_{TR}$ signature**
318 The relative contributions to the $\delta^{18}O_{TR}$ signature of the isotopic signal of the source (xylem)
319 water and of the ^{18}O enrichment of the leaf water due to transpiration were investigated. In both
320 regions, the Leaf water enrichment experimental simulations and the reference simulations have a
321 higher correlation coefficient (R^2 centred on 0.9 and 0.95, respectively for northeastern Canada
322 and western Argentina; Figure 5) than are the XW source simulations with the reference
323 simulations (R^2 centred on 0.65 and 0.8, respectively for northeastern Canada and western
324 Argentina). This suggests that, with the model, the variability of $\delta^{18}O_{XW}$ has a weaker influence
325 on $\delta^{18}O_{TR}$ variations than the changes of the leaf water isotopic enrichment do. Notably, *P.*
326 *mariana* in northeastern Canada appears to be more sensitive to both influences than *N. pumilio*
327 in western Argentina (Figure 5).

328

329 **4. DISCUSSION**
330 **4.1. Precipitation $\delta^{18}O_P$ variations and estimation**

331   Although the regression models used to predict daily $\delta^{18}O_P$ values are likely too simplistic, the

332   resultant monthly averaged values adequately reproduce the distribution of the observed (from

333   GNIP stations) and modelled (by GCMs) monthly $\delta^{18}O_P$ series in northeastern Canada. In

334   western Argentina, the distribution of monthly $\delta^{18}O_P$ values is also well reproduced but the

335   amplitude of variation of the predicted values is too high, leading to simulated values lower than

336   the measured ones during the colder months. The temporal $\delta^{18}O_P$ variations are positively related

337   to air temperature given the positive coefficient *a*. In agreement with the simple Rayleigh

338   distillation model (Dansgaard, 1964), as air temperature decreases, the specific humidity at

339   saturation decreases, and water vapour condenses. $H_2^{18}O$ condenses preferentially, the residual

340   water vapour gets more and more depleted as condensation proceeds. Consequently, in the

341   Tropics, the $^{18}O/^{16}O$ ratio in the meteoric water has been observed to decrease with increasing

342   amount of precipitation and/or relative humidity (Rozanski et al., 1993). In extra-tropical regions,

343    $\delta^{18}O_P$ may also correlate with precipitation amount (negative coefficient *b*), since both variables

344   depend on the meteorological conditions.

345   The results of the linear regressions show comparatively lower influence of precipitation on

346    $\delta^{18}O_P$ in western Argentina than in northeastern Canada (Table 1). This suggests that the imprint

347   of the precipitation amount on $\delta^{18}O_P$ in western Argentina is low and that $\delta^{18}O_P$ variations are

348   mainly controlled by seasonal changes in temperature, which is in agreement with previous work

349   (Rozanski et al., 1995). However, due to the strong west-to-east precipitation gradient in this

350   region (orographic rain shadow), large $\delta^{18}O_P$ variations occur over short distances (Rozanski et

351   al., 1995; Smith and Evans, 2007; Stern and Blisniuk, 2002). Therefore, the daily precipitation

352   dataset extracted from the gridded reanalysis data, which has a low spatial resolution (>200 km),

353   may not represent the daily variations in precipitation at a local scale faithfully. Therefore, the

354   model may underestimate the contribution of precipitation on $\delta^{18}O_P$ variability in this particular

355   area.

356

357   In contrast, in northeast Canada, both temperature and precipitation amount equally control the

358    $\delta^{18}O_P$ variations. The high amount of precipitation falling in summer (~46%) should have a

359   strong effect and decrease the $\delta^{18}O_P$ values in the condensed water, while high temperatures

360   counteract this effect by increasing this ratio. Before reaching northeastern Canada, the air

361   masses pushed by the dominant westerly winds discharge most of their humidity over the land,

362   leading to a depleted $\delta^{18}O_P$ signal at our sites (for the same reason, $\delta^{18}O_{TR}$ values at L20, which is

363   located 110 km North-East of L01, are ~1‰ lower). Moreover, the $\delta^{18}O_P$ signal in the Canadian

364   sites is comparatively more depleted than in the Argentinian sites, because of their higher

365   latitude. It is worth noting that the resolution of the gridded meteorological dataset used for the

366   Canadian sites is relatively high (~10 km), which means that the local processes are likely well

367   represented.

368

369   **4.2. Relative performance in modelling $\delta^{18}O_{TR}$ values**

370   The simulated $\delta^{18}O_{TR}$ series based on daily $\delta^{18}O_P$ estimation from the regression models

371   reproduce the observations better than the ones based on $\delta^{18}O_P$ values derived from GCMs

372   (Figure 4). This is in part due to the greater number of parameters to optimize, as the calibration

373   process can more easily find a solution that fits the observations better. This may however reflect

374   error compensations especially in western Argentina where the estimated annual variability of

375    $\delta^{18}O_P$ is too large. Conversely in northeastern Canada, the annual variations of $\delta^{18}O_P$ that are

376   estimated, simulated by GCMs and observed are in good agreement (Figure SM2). Although

377   isotope-enabled atmospheric global models can reproduce the mean annual precipitation isotopic

378   values and seasonality for many areas (Risi et al., 2010), results at specific sites, especially in

379   mountainous regions such as at our western Argentinian site, can be less accurate (Figure SM2;

380   see the offset between GNIP stations and LMDZ-NCEP20). Ideally, daily $\delta^{18}O_P$ long-term

381   records from meteorological stations in the study region should be used as an input of

382   MAIDENiso. Simulations from high-resolution regional circulation models, such as REMOiso

383   which has a 0.5°×0.5° (~55 km) horizontal resolution (Insel et al., 2013; Sturm et al., 2007,

384   2005), may produce reliable local $\delta^{18}O_P$ values. Such dataset has proven to be quite helpful with

385   MAIDENiso in the Fontainebleau forest (France) (Danis et al., 2012). However, up to now,

386   measured or REMOiso $\delta^{18}O_P$ datasets in our regions of study do not exist, which is the case for

387   most regions of the world. Moreover, early data (1970-80s) from GNIP stations may have been

388   compromised by pan evaporation and therefore isotopic enrichment. Therefore, we recommend

389   that daily GNIP stations are set up in various forested ecosystems, that an effort is accomplished

390   to homogenize older GNIP time series, and that high resolution simulations of $\delta^{18}O_P$ are

391   performed in wider regions.

392

393   The modelling of $\delta^{18}O_{TR}$ values based on the estimation of $\delta^{18}O_P$ is relatively more accurate for

394   northeastern Canada than for western Argentina (Figure 3). As the mean levels of the measured

395    $\delta^{18}O_{TR}$ values are high at the western Argentinian sites (mean value of about 30‰), the Bayesian

396   optimization tends to increase the biochemical (ε_0) and kinetic (ε_k) fractionations as well as the

397   coefficient a, while reducing the dampening factor (f_o) to reach more representative mean levels

398   of the $\delta^{18}O_{TR}$ simulation. But still, these levels are too low in comparison with the observations

399   (about 2.5‰ lower; Figure SM4). When the posterior value of a calibrated parameter is limited to

400   the upper bound of the prior range of plausible values, as it is the case at the western Argentinian

401   sites for a, b and ε_0 (Figure SM3), it means that either the prior range is too narrow, or the model

402   is inadequate, or some important process is not considered in the model. Here, the estimation of

403   the prior ranges of both coefficients a and b were based on observed (GNIP stations) and

404   simulated (GCMs) $\delta^{18}O_P$ values. Therefore, we expect their respective ranges to be consistent

405   with local processes. When the prior range of a is extended to higher values in the optimization

406   process, observed and simulated $\delta^{18}O_{TR}$ mean levels in western Argentina are better matching.

407   However, in this case, the distribution of $\delta^{18}O_P$ values is shifted toward higher values, advocating

408   for unrealistic estimated $\delta^{18}O_P$ variations.

409   One other possibility is that the prior range of ε_0 is too narrow. In accordance with DeNiro and

410   Epstein (1981), Sternberg (1989) and Yakir and DeNiro (1990), the biochemical fractionation ε_0

411   is assumed here to be lower than 30‰. However, a recent study has demonstrated that this

412   parameter, nearly constant between 20 to 30°C, increases at lower temperatures to values of 31‰

413   (Sternberg and Ellsworth, 2011). During the growing season, maximum temperatures can reach

414   20°C in western Argentina and 30°C in northeastern Canada, which suggests that the high mean

415    $\delta^{18}O_{TR}$ levels in *N. pumilio* may be due to biochemical fractionation higher than 30‰ due to

416   temperature generally lower than 20°C. However, when the prior range of ε_0 is extended to 31‰

417   in the optimization process, the mean $\delta^{18}O_{TR}$ levels of *N. pumilio* are still too low in comparison

418   with the observations. These results advocate for the existence of other processes, which can

419   explain this offset in mean levels in Argentina. For example, higher soil water evaporation than

420   modelled by MAIDENiso should lead to less negative $\delta^{18}O_{SW}$ (and therefore $\delta^{18}O_{XW}$), which

421   could explain the high mean levels of $\delta^{18}O_{TR}$ in Argentina. Caution should be exercised with such

422   an interpretation since other species living in similar conditions as *N. pumilio* in western

423   Argentina show comparatively lower mean $\delta^{18}O_{TR}$ levels than *N. pumilio* (i.e., *Fitzroya*

424 *cupressoides*; see Lavergne et al., 2016). The ongoing monitoring and evaluation of isotopic
425 processes based on synchronous measurements of vapour, precipitation, soil water and xylem
426 water will certainly help understanding the high mean levels observed in Argentina, and
427 increasing the representation of the involved processes in MAIDENiso.

428

429 The better fit between observed and simulated $\delta^{18}O_{TR}$ values obtained with specific forms of
430 synthetic distributions of daily GPP for northeastern Canada and western Argentina (Figure 3)
431 suggests differential limiting factors in the two regions. The synthetic bimodal distribution of
432 daily GPP with maxima in spring and autumn, as simulated in western Argentina, is often
433 observed in a diversity of ecosystems such as in the Mediterranean environments (Baldocchi et
434 al., 2010; Gea-Izquierdo et al., 2015). After the activation of the photosynthesis in early spring,
435 increasing temperatures tend to be optimal for tree growth. However, in a modelling study,
436 Lavergne et al. (2015) have shown that the influence of temperature on *N. pumilio*'s growth
437 becomes negative once a temperature threshold (soil moisture) is exceeded. Therefore, we
438 assume that after reaching a threshold of temperature and soil moisture summer conditions, tree
439 growth is inhibited, leading to a decrease of primary productivity. However, when temperature
440 starts to decline and soil water supply tends to increase with increasing precipitation events, tree
441 growth increases again until the end of the growing season. In contrast, because precipitation is
442 more abundant in summer (June to September) in northeastern Canada (Naulier et al., 2014), high
443 summer temperatures should be always beneficial to tree growth if enough soil water is available.
444 Therefore, in agreement with GPP-derived eddy covariance data from the Fluxnet network (see
445 Gennaretti et al., 2017a), a better fit between observations and simulations is observed when
446 using a unimodal rather than a bimodal GPP distribution. Monitoring of tree physiology,
447 environmental conditions and wood cell formation will provide a more detailed representation of
448 the complex biological and ecological processes operating in Patagonia, allowing us to run the
449 MAIDENiso model with better constraints.

450

451 **4.3. What is the main origin of the temperature signal recorded in $\delta^{18}O_{TR}$?**

452 The investigation of the relative contributions of the isotopic composition of the source (xylem)
453 water and of the ^{18}O enrichment of the leaf water by transpiration on the simulated $\delta^{18}O_{TR}$ reveals
454 that the variability of the former has a weaker influence on $\delta^{18}O_{TR}$ variations than that of the

455 latter in North and South America. Therefore, the temperature signal recorded in $\delta^{18}O_{TR}$ series

456 more likely reflects the effect of temperature on isotopic enrichment of the leaf water rather than

457 on the isotopic composition of the source water. At the leaf-level, air temperature has a strong

458 effect on the relative humidity and therefore on the vapour pressure deficit (VPD), i.e. the

459 difference between the saturation vapour pressure and the actual vapour pressure, which

460 modulates the transpiration (Barbour, 2007). Thus, the imprint of the ambient air temperature on

461 the fractionation processes occurring during transpiration is preferentially recorded in the tree

462 rings of the two species. Furthermore, both the isotopic signature of the xylem water and of the

463 fractionation processes occurring at the evaporation sites of the leaves have comparatively higher

464 influence on $\delta^{18}O_{TR}$ in *P. mariana* than in *N. pumilio*. This is probably due to the lower amplitude

465 of the day-by-day variations of the relative humidity in western Argentina (SD = 5%) versus in

466 northeastern Canada (SD = 16%) that translates into a weaker influence of h_{air} variations and

467 therefore of leaf-level isotopic fractionation processes on $\delta^{18}O_{TR}$ values in western Argentina

468 than in northeastern Canada. These results highlight the potential of MAIDENiso model to better

469 refine the origin of the climatic signal recorded in the oxygen isotopic signature in the tree rings

470 of different species.

471

472 **5. CONCLUSION**

473 Here, by using MAIDENiso model, we have provided a mechanistic overview of the climatic and

474 biological processes controlling oxygen isotopic fractionation in two American temperature-

475 sensitive tree species. First, we have shown that using regression-based rather than model-based

476 $\delta^{18}O_P$ estimates as inputs increases the predictive skills of our simulations, although this may be

477 at the price of error compensations. Second, our study reveals that the variability of the isotopic

478 composition of the source (xylem) water has a weaker influence on $\delta^{18}O_{TR}$ variations than that of

479 the ^{18}O enrichment of the leaf water by transpiration. Last, these findings suggest that the imprint

480 of temperature recorded in $\delta^{18}O_{TR}$ of the two species is likely related to the effect of temperature

481 on isotopic enrichment of the leaf water. The isotopic monitoring of water within the soil-

482 vegetation-atmosphere compartments in future work will certainly provide the input and control

483 data necessary to better constrain MAIDENiso. Our study demonstrates that the eco-

484 physiological modelling of $\delta^{18}O_{TR}$ values is necessary and likely the only approach to accurately

485 interpret the recorded climate signal. Based on the calibrations of MAIDENiso presented here,

486 the next step involves inverse modelling approaches to perform paleoclimatic reconstructions in
487 North and South America that are less biased by the complex and nonlinear interactions between
488 climate, CO_2 concentrations and tree growth as recommended by Boucher et al. (2014).
489

490 **Code and data availability**
491 The code of the model can be found in https://doi.org/10.6084/m9.figshare.5446435.v1. The daily
492 $\delta^{18}O_P$ data from the MUGCM model were extracted via the SWING project webpage
493 (http://paos.colorado.edu/~dcn/SWING/database.php). The daily climatic data used for Quebec
494 were retrieved from http://cfs.nrcan.gc.ca/projects/3/4, while those for Argentina were extracted
495 from https://www.esrl.noaa.gov/psd/data/gridded/data.20thC_ReanV2c.html. The atmospheric
496 CO_2 concentration data derived from the Mauna Loa station were extracted from
497 http://www.esrl.noaa.gov/gmd/ccgg/trends/.

498

499 **ACKNOWLEDGMENTS**
500 This study has been co-funded by the Research Federation ECCOREV. A.L. has been supported
501 by a Research associate/Lecturer position at the Aix-Marseille University (France). F.G. has
502 received funding from the European Union's Horizon 2020 research and innovation program
503 under the Marie Sklodowska-Curie grant agreement No 656896. We acknowledge all data
504 providers: the Instituto Argentino de Nivología, Glaciología y Ciencias Ambientales (IANIGLA,
505 Argentina) for providing the daily temperature data from La Almohadilla site; the National
506 Meteorological Service from Argentina for providing the monthly temperature data from
507 Bariloche meteorological station (Argentina); the Department of Natural Resources Canada for
508 providing the daily climatic data used for Quebec; the US Department of Energy, Office of
509 Science Biological and Environmental Research (BER) and the National Oceanic and
510 Atmospheric Administration Climate Program Office for providing the daily climatic data used
511 for Argentina; and the SWING project for providing the daily $\delta^{18}O_P$ data from MUGCM model.

512

513 # References

514 Baldocchi, D. D., Ma, S., Rambal, S., Misson, L., Ourcival, J. M., Limousin, J. M., Pereira, J. and
515 Papale, D.: On the differential advantages of evergreenness and deciduousness in mediterranean
516 oak woodlands: A flux perspective, Ecol. Appl., 20(6), 1583–1597, doi:10.1890/08-2047.1, 2010.

517   Barbour, M. M.: Stable oxygen isotope composition of plant tissue: a review, Funct. Plant Biol.,

518   34, 83–94, doi:10.1071/FP06228, 2007.

519   Barbour, M. M., Cernusak, L. A. and Farquhar, G. D.: Factors affecting the oxygen isotope ratio

520   of plant organic material, in Stable isotopes and biosphere-atmosphere interactions: Processes

521   and Biological Controls, edited by L. B. Flanagan, J. R. Ehleringer, and D. E. Pataki, pp. 9–28,

522   Elsevier, Amsterdam., 2005.

523   Boucher, E., Guiot, J., Hatté, C., Daux, V., Danis, P. A. and Dussouillez, P.: An inverse modeling

524   approach for tree-ring-based climate reconstructions under changing atmospheric CO_2

525   concentrations, Biogeosciences, 11(12), 3245–3258, 2014.

526   Brienen, R. J. W., Helle, G., Pons, T. L., Guyot, J.-L. and Gloor, M.: Oxygen isotopes in tree

527   rings are a good proxy for Amazon precipitation and El Niño-Southern Oscillation variability,

528   Proc. Natl. Acad. Sci., 109(42), 16957–16962, doi:10.1073/pnas.1205977109, 2012.

529   Buhay, W. M., Edwards, T. W. D. and Aravena, R.: Evaluating kinetic fractionation factors used

530   for reconstructions from oxgen and hydrogen isotope ratios in plant water and cellulose,

531   Geochemistry, Geophys. Geosystems, 60(12), 2209–2218, 1996.

532   Cernusak, L. A. and English, N. B.: Beyond tree-ring widths: stable isotopes sharpen the focus on

533   climate responses of temperate forest trees, Tree Physiol., 35(1), 1–3,

534   doi:10.1093/treephys/tpu115, 2015.

535   Compo, G. P., Whitaker, J. S., Sardeshmukh, P. D., Matsui, N., Allan, R. J., Yin, X., Gleason, B.

536   E., Vose, R. S., Rutledge, G., Bessemoulin, P., BroNnimann, S., Brunet, M., Crouthamel, R. I.,

537   Grant, A. N., Groisman, P. Y., Jones, P. D., Kruk, M. C., Kruger, A. C., Marshall, G. J., Maugeri,

538   M., Mok, H. Y., Nordli, O., Ross, T. F., Trigo, R. M., Wang, X. L., Woodruff, S. D. and Worley,

539   S. J.: The twentieth century reanalysis project, Q. J. R. Meteorol. Soc., 137(654), 1–28,

540   doi:10.1002/qj.776, 2011.

541   Craig, H. and Gordon, L. I.: Deuterium and oxygen 18 variations in the ocean and the marine

542   atmosphere, Spoleto, 1965.

543   Danis, P. A., Hatté, C., Misson, L. and Guiot, J.: MAIDENiso: a multiproxy biophysical model of

544   tree-ring width and oxygen and carbon isotopes, Can. J. For. Res., 42(9), 1697–1713,

545   doi:10.1139/x2012-089, 2012.

546   Danis, P. A., Masson-Delmotte, V., Stievenard, M., Guillemin, M. T., Daux, V., Naveau, P. and

547   von Grafenstein, U.: Reconstruction of past precipitation $\delta^{18}O$ using tree-ring cellulose $\delta^{18}O$ and

548 δ^{13}C: A calibration study near Lac d'Annecy, France, Earth Planet. Sci. Lett., 243(3–4), 439–448,

549 doi:10.1016/j.epsl.2006.01.023, 2006.

550 Dansgaard, W.: Stable isotopes in precipitation, Tellus A, 16(4), 436–468,

551 doi:10.3402/tellusa.v16i4.8993, 1964.

552 DeNiro, M. J. and Epstein, S.: Relationship between the oxygen isotope ratios of terrestrial plant

553 cellulose, carbon dioxide, and water, Science, 204, 51-53, 1979.

554 DeNiro, M. J. and Epstein, S.: Isotopic composition of cellulose from aquatic organisms,

555 Geochim. Cosmochim. Acta, 45(10), 1885–1894, doi:10.1016/0016-7037(81)90018-1, 1981.

556 Donoso, C.: Tipos forestales de los bosques nativos de Chile., Documento de Trabajo Nu. 38.

557 Investigación y Desarrollo Forestal (CONAF, PNUD-FAO). FAO Chile., 1981.

558 Farquhar, G. D., Barbour, M. M. and Henry, B. K.: Interpretation of oxygen isotope composition

559 of leaf material, in Stable isotopes: integration of biological, ecological and geochemical

560 processes, pp. 27–61, BIOS Scientific Publishers: Oxford., 1998.

561 Farquhar, G. D., Hubick, H. T., Condon, A. G. and Richards, R. A.: Carbon isotope fractionation

562 and plant water-use efficiency, in Stable isotopes in ecological research, pp. 21–40., 1989.

563 Gea-Izquierdo, G., Guibal, F., Joffre, R., Ourcival, J. M., Simioni, G. and Guiot, J.: Modelling

564 the climatic drivers determining photosynthesis and carbon allocation in evergreen Mediterranean

565 forests using multiproxy long time series, Biogeosciences, 12(12), 3695–3712, doi:10.5194/bg-

566 12-3695-2015, 2015.

567 Gennaretti, F., Arseneault, D., Nicault, A., Perreault, L. and Bégin, Y.: Volcano-induced regime

568 shifts in millennial tree-ring chronologies from northeastern North America., Proc. Natl. Acad.

569 Sci. U. S. A., 111(28), 10077-10082, doi:10.1073/pnas.1324220111, 2014.

570 Gennaretti, F., Gea-Izquierdo, G., Boucher, E., Berninger, F., Arseneault, D. and Guiot, J.:

571 Ecophysiological modeling of the climate imprint on photosynthesis and carbon allocation to the

572 tree stem in the North American boreal forest, Biogeosciences Discuss., in review,

573 doi:10.5194/bg-2017-51, 2017a.

574 Gennaretti, F., Huard, D., Naulier, M., Savard, M., Bégin, C., Arseneault, D. and Guiot, J.:

575 Bayesian multiproxy temperature reconstruction with black spruce ring widths and stable

576 isotopes from the northern Quebec taiga, Clim. Dyn., 1–13, doi:10.1007/s00382-017-3565-5,

577 2017b.

578 Gessler, A., Ferrio, J. P., Hommel, R., Treydte, K., Werner, R. A. and Monson, R. K.: Stable

579   isotopes in tree rings: towards a mechanistic understanding of isotope fractionation and mixing

580   processes from the leaves to the wood., Tree Physiol., 0, 1–23, 2014.

581   Guiot, J., Boucher, E. and Gea-Izquierdo, G.: Process models and model-data fusion in

582   dendroecology, Front. Ecol. Evol., 2, 52, doi:10.3389/fevo.2014.00052, 2014.

583   Hartl-Meier, C., Zang, C., Büntgen, U. L. F., Esper, J. A. N., Rothe, A., Göttlein, A., Dirnböck,

584   T. and Treydte, K.: Uniform climate sensitivity in tree-ring stable isotopes across species and

585   sites in a mid-latitude temperate forest., Tree Physiol., 2003(1), 4–15,

586   doi:10.1093/treephys/tpu096, 2014.

587   Helliker, B. R. and Richter, S. L.: Subtropical to boreal convergence of tree-leaf temperatures,

588   Nature, 454(7203), 511–514, doi:10.1038/nature07031, 2008.

589   Horita, J. and Wesolowski, D. J.: Liquid-vapor fractionation of oxygen and hydrogen isotopes of

590   water from the freezing to the critical temperature, Geochim. Cosmochim. Acta, 58(16), 3425–

591   3437, doi:10.1016/0016-7037(94)90096-5, 1994.

592   Hourdin, F., Grandpeix, J. Y., Rio, C., Bony, S., Jam, A., Cheruy, F., Rochetin, N., Fairhead, L.,

593   Idelkadi, A., Musat, I., Dufresne, J. L., Lahellec, A., Lefebvre, M. P. and Roehrig, R.: LMDZ5B:

594   The atmospheric component of the IPSL climate model with revisited parameterizations for

595   clouds and convection, Clim. Dyn., 40(9–10), 2193–2222, doi:10.1007/s00382-012-1343-y,

596   2013.

597   Hutchinson, M. F., McKenney, D. W., Lawrence, K., Pedlar, J. H., Hopkinson, R. F., Milewska,

598   E. and Papadopol, P.: Development and testing of Canada-wide interpolated spatial models of

599   daily minimum-maximum temperature and precipitation for 1961-2003, J. Appl. Meteorol.

600   Climatol., 48(4), 725–741, doi:10.1175/2008JAMC1979.1, 2009.

601   Insel, N., Poulsen, C. J., Sturm, C. and Ehlers, T. A.: Climate controls on Andean precipitation

602   δ^{18}O interannual variability, J. Geophys. Res. Atmos., 118(17), 9721–9742,

603   doi:10.1002/jgrd.50619, 2013.

604   Kahmen, A., Sachse, D., Arndt, S. K., Tu, K. P., Farrington, H., Vitousek, P. M. and Dawson, T.

605   E.: Cellulose δ^{18}O is an index of leaf-to-air vapor pressure difference (VPD) in tropical plants.,

606   Proc. Natl. Acad. Sci. U. S. A., 108(5), 1981–1986, doi:10.1073/pnas.1018906108, 2011.

607   Keeling, C. D., Bacastow, R. B., Bainbridge, A. E., Ekdahl Jr., C. A., Guenther, P. R.,

608   Waterman, L. S. and Chin, J. F. S.: Atmospheric carbon dioxide variations at Mauna Loa

609   Observatory, Hawaii, Tellus A, 28, 538–551, doi:10.3402/tellusa.v28i6.11322, 1976.

610   Labuhn, I., Daux, V., Girardclos, O., Stievenard, M., Pierre, M. and Masson-Delmotte, V.:

611   French summer droughts since 1326 AD: a reconstruction based on tree ring cellulose δ^{18}O,

612   Clim. Past, 11(6), 5113–5155, doi:10.5194/cpd-11-5113-2015, 2016.

613   Lavergne, A., Daux, V., Villalba, R. and Barichivich, J.: Temporal changes in climatic limitation

614   of tree-growth at upper treeline forests: Contrasted responses along the west-to-east humidity

615   gradient in Northern Patagonia, Dendrochronologia, 36, 49–59, 2015.

616   Lavergne, A., Daux, V., Villalba, R., Pierre, M., Stievenard, M. and Srur, A. M.: Improvement of

617   isotope-based climate reconstructions in Patagonia through a better understanding of climate

618   influences on isotopic fractionation in tree rings, Earth Planet. Sci. Lett., 459, 372–380,

619   doi:10.1016/j.epsl.2016.11.045, 2017.

620   Lavergne, A., Daux, V., Villalba, R., Pierre, M., Stievenard, M., Srur, A. M. and Vimeux, F.: Are

621   the δ^{18}O of F. cupressoides and N. pumilio promising proxies for climate reconstructions in

622   northern Patagonia?, J. Geophys. Res. - Biogeosciences, 121(3), 767–776,

623   doi:10.1002/2015JG003260, 2016.

624   López Bernal, P., Defossé, G. E., Quinteros, C. P. and Bava, J. O.: Sustainable management of

625   lenga (Nothofagus pumilio) forests through group selection system, in Sustainable forest

626   management - current research, edited by D. J. J. D. (Ed.), pp. 45–66, 2012.

627   Lorrey, A. M., Brookman, T. H., Evans, M. N., Fauchereau, N.C., Barbour, M., Macinnis-Ng, C.

628   Criscitiello, A., Eischeid, G., Fowler, A. M., Horton, T. W. and Schrag, D. P.: Stable oxygen

629   isotope signatures of early season wood in New Zealand kauri (Agathis australis) tree rings:

630   Prospects for palaeoclimate reconstruction., Dendrochronologia, 40, 50–63, doi:

631   10.1016/j.dendro.2016.03.012, 2016.

632   Magnin, A., Puntieri, J. and Villalba, R.: Interannual variations in primary and secondary growth

633   of Nothofagus pumilio and their relationships with climate, Trees, 28(5), 1463–1471, 2014.

634   Misson, L.: MAIDEN: a model for analyzing ecosystem processes in dendroecology, Can. J. For.

635   Res., 34, 874–887, 2004.

636   Naulier, M., Savard, M. M., Bégin, C., Gennaretti, F., Arseneault, D., Marion, J., Nicault, A. and

637   Bégin, Y.: A millennial summer temperature reconstruction for northeastern Canada using

638   oxygen isotopes in subfossil trees, Clim. Past, 11(9), 1153–1164, doi:10.5194/cp-11-1153-2015,

639   2015.

640   Naulier, M., Savard, M. M., Bégin, C., Marion, J., Arseneault, D. and Bégin, Y.: Carbon and

641   oxygen isotopes of lakeshore black spruce trees in northeastern Canada as proxies for climatic

642   reconstruction, Chem. Geol., 374–375, 37–43, doi:10.1016/j.chemgeo.2014.02.031, 2014.

643   Noone, D. and Simmonds, I.: Associations between $\delta^{18}O$ of water and climate parameters in a

644   simulation of atmospheric circulation for 1979–95, J. Clim., 15, 3150–3169, 2002.

645   Ogée, J., Barbour, M. M., Wingate, L., Bert, D., Bosc, A., Stievenard, M., Lambrot, C., Pierre,

646   M., Bariac, T., Loustau, D. and Dewar, R. C.: A single-substrate model to interpret intra-annual

647   stable isotope signals in tree-ring cellulose, Plant, Cell Environ., 32(8), 1071–1090,

648   doi:10.1111/j.1365-3040.2009.01989.x, 2009.

649   Ogée, J., Brunet, Y., Loustau, D., Berbigier, P. and Delzon, S.: MuSICA, a CO_2, water and

650   energy multilayer, multileaf pine forest model: Evaluation from hourly to yearly time scales and

651   sensitivity analysis, Glob. Chang. Biol., 9(5), 697–717, doi:10.1046/j.1365-2486.2003.00628.x,

652   2003.

653   Rinne, K. T., Loader, N. J., Switsur, V. R. and Waterhouse, J. S.: 400-year May-August

654   precipitation reconstruction for Southern England using oxygen isotopes in tree rings, Quat. Sci.

655   Rev., 60, 13–25, doi:10.1016/j.quascirev.2012.10.048, 2013.

656   Risi, C., Bony, S., Vimeux, F. and Jouzel, J.: Water-stable isotopes in the LMDZ4 general

657   circulation model: Model evaluation for present-day and past climates and applications to

658   climatic interpretations of tropical isotopic records, J. Geophys. Res. Atmos., 115(12), 1–27,

659   doi:10.1029/2009JD013255, 2010.

660   Roden, J. S., Lin, G. and Ehleringer, J. R.: A mechanistic model for interpretation of hydrogen

661   and oxygen isotope ratios in tree-ring cellulose, Geochim. Cosmochim. Acta, 64(1), 21–35,

662   doi:10.1016/S0016-7037(99)00195-7, 2000.

663   Rozanski, K., Araguás-Araguás, L.: Spatial and temporal variability of stable isotope

664   composition of precipitation over the South American continent, Bull. l'Institut Fr. d'études

665   Andin., 24(3), 379–390, 1995.

666   Rozanski, K., Araguás-Araguás, L. and Gonfiantini, R.: Isotopic patterns in modern global

667   precipitation, in Climate change in continental isotopic records., edited by P. K. Swart, K. C.

668   Lohmann, J. McKenzie, and S. Savin, American Geophysical Union., 1993.

669   Running, S. W., Nemani, R. R. and Hungerford, R. D.: Extrapolation of synoptic meteorological

670   data in mountainous terrain and its use for simulating forest evapotranspiration and

671   photosynthesis, Can. J. For. Res., 17, 472–483, doi:10.1139/x87-081, 1987.

672   Rusch, V. E.: Altitudinal variation in the phenology of Nothofagus pumilio in Argentina, Rev.

673   Chil. Hist. Nat., 66(2), 131–141, 1993.

674   Saurer, M., Aellen, K. and Siegwolf, R. T. W.: Correlating $\delta^{13}C$ and $\delta^{18}O$ in cellulose of trees,

675   Plant, Cell Environ., 20, 1543–1550, 1997.

676   Saurer, M., Cherubini, P., Reynolds-Henne, C. E., Treydte, K. S., Anderson, W. T. and Siegwolf,

677   R. T. W.: An investigation of the common signal in tree ring stable isotope chronologies at

678   temperate sites, J. Geophys. Res. Biogeosciences, 113(4), doi:10.1029/2008JG000689, 2008.

679   Schlatter, J.: Requerimientos de sitio para la lenga, Nothofagus pumilio (Poepp. et Endl.) Krasser,

680   Bosque, 15, 3–10, 1994.

681   Shi, C., Daux, V., Zhang, Q. B., Risi, C., Hou, S. G., Stievenard, M., Pierre, M., Li, Z. and

682   Masson-Delmotte, V.: Reconstruction of southeast Tibetan Plateau summer climate using tree

683   ring $\delta^{18}O$: Moisture variability over the past two centuries, Clim. Past, 8(1), 205–213,

684   doi:10.5194/cp-8-205-2012, 2012.

685   Smith, R. B. and Evans, J. P.: Orographic precipitation and water vapor fractionation over the

686   Southern Andes, J. Hydrometeorol., 8(1), 3–19, doi:10.1175/JHM555.1, 2007.

687   Stern, L. A. and Blisniuk, P. M.: Stable isotope composition of precipitation across the southern

688   Patagonian Andes, J. Geophys. Res. Atmos., 107(23), doi:10.1029/2002JD002509p, 2002.

689   Sternberg, L. D. S. L.: Oxygen and hydrogen isotope ratios in plant cellulose: Mechanisms and

690   applications, in Stable isotopes in ecological research, edited by J. R. E. and K. A. N. P. W.

691   Rundel, pp. 124–141., 1989.

692   Sternberg, L. D. S. L. and Ellsworth, P. F. V.: Divergent biochemical fractionation, not

693   convergent temperature, explains cellulose oxygen isotope enrichment across latitudes, PLoS

694   One, 6(11), e28040, doi:10.1371/journal.pone.0028040, 2011.

695   Sturm, C., Vimeux, F. and Krinner, G.: Intraseasonal variability in South America recorded in

696   stable water isotopes, J. Geophys. Res. Atmos., 112(20), doi:10.1029/2006JD008298, 2007.

697   Sturm, K., Hoffmann, G., Langmann, B. and Stichler, W.: Simulation of $\delta^{18}O$ in precipitation by

698   the regional circulation model REMOiso, Hydrol. Process., 19(17), 3425–3444,

699   doi:10.1002/hyp.5979, 2005.

700   Treydte, K., Boda, S., Graf Pannatier, E., Fonti, P., Frank, D., Ullrich, B., Saurer, M., Siegwolf,

701   R. T. W., Battipaglia, G., Werner, W. and Gessler, A.: Seasonal transfer of oxygen isotopes from

702   precipitation and soil to the tree ring: Source water versus needle water enrichment, New Phytol.,

703   202(3), 772–783, doi:10.1111/nph.12741, 2014.

704   Viereck, L. A. and Johnston, W. F.: Picea mariana (Mill.) B. S. P., in Silvics of North America:

705   1. Conifers; 2. Hardwoods., edited by R. M. Burns and B. H. Honkala, pp. 443–464, US.

706   Department of Agriculture, Forest Service, Washington, DC., 1990.

707   Wernicke, J., Grießinger, J., Hochreuther, P. and Braüning, A.: Variability of summer humidity

708   during the past 800 years on the eastern Tibetan Plateau inferred from $\delta^{18}O$ of tree-ring cellulose.,

709   Clim. Past, 11, 327–337, doi:10.5194/cp-11-327-2015, 2015.

710   Wershaw, R. L., Friedman, I. and Heller, S. J.: Hydrogen isotope fractionation in water passing

711   through trees, in Advances in Organic Geochemistry, edited by F. Hobson and M. Speers, pp. 55–

712   67, New York, Pergamon., 1966.

713   Yakir, D. and DeNiro, M. J.: Oxygen and hydrogen isotope fractionation during cellulose

714   metabolism in lemna gibba L., Plant Physiol., 93(1), 325–332, doi:10.1104/pp.93.1.325, 1990.

715

716

Tables and Figures

718

719 **Table 1** Definition of sensitive parameters. The posterior medians and 90% confidence intervals

720 are also shown.

721

Parameter	Definition	Unit	Parameter type (prior range)	Values with 90% posterior confidence intervals
f_o	Dampening factor	NA	Calibrated (0.3 to 0.5)	0.36 [0.31; 0.46] (Arg.) 0.41 [0.32; 0.48] (Q.)
ε_0	Biochemical fractionation	‰	Calibrated (24 to 30)	29.99 [29.93; 30] (Arg.) 26.81 [24.74; 28.04] (Q.)
ε_k	Kinetic fractionation	‰	Calibrated (10 to 30)	28.86 [18.25; 29.96] (Arg.) 17.20 [11.16; 26.34] (Q.)
a	Temperature dependence of $\delta^{18}O_P$	NA	Calibrated (0.2 to 0.5 for Arg. and 0 to 0.38 for Q.)	0.50 [0.49; 0.50] (Arg.) 0.31 [0.25; 0.37] (Q.)
b	Precipitation dependence of $\delta^{18}O_P$	NA	Calibrated (-0.3 to 0 for Arg. and -0.39 to 0 for Q.)	-0.009 [-0.15; 0] (Arg.) -0.22 [-0.35; -0.14] (Q.)
c	Intercept of $\delta^{18}O_P$	‰	Fixed	-10.0 (Arg.) -11.9 (Q.)

722
723
724
725

726   **Table 2** Climate input data for all tested simulations
727

	Daily Tmin and Tmax	**Daily P**	**Daily $\delta^{18}O_P$**	**CO$_2$**
Configuration 1	Canadian database/ NOAA-CIRES dataset		Linear regression	Mauna
Configuration 2	Canadian database / NOAA-CIRES dataset	MUGCM data		Loa
Configuration 3	LMDZ-NCEP20 data			station

728
729

730   **Figure 1** Tree ring δ¹⁸O time series (‰) at the three sites in Argentina (NUB, ALM and CHA in

731   dark grey) and two sites in Quebec (L01 and L20 in dark grey; single trees in light grey). The

732   bold black lines are the averaged values. The mean inter-site correlation coefficients are

733   r = 0.60, p < 0.05 and r = 0.80, p < 0.01 in the South and North American sites, respectively.

734

735

736
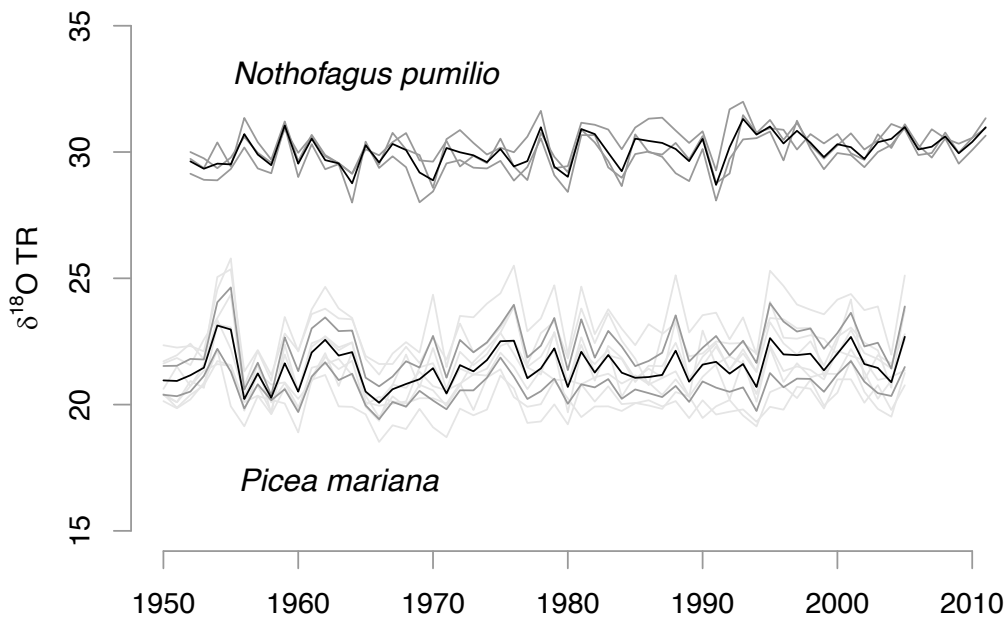
737 **Figure 2** Dependence of the correlation coefficients between observed and simulated $\delta^{18}O_{TR}$

738 series (panels A), and of the mean simulated $\delta^{18}O_{TR}$ levels (‰) (panels B) as a function of the

739 range of calibrated parameters a, b, f_o, ε_0 and ε_k for the 50 simulations performed. The tests sites

740 from Quebec are in black and the Argentinean ones are in red. The vertical lines are the values of

741 a plausible block of parameters retained in the MCMC optimization. The horizontal dashed lines

742 are their respective 90% confidence interval calculated with 50 simulations (see Table 1). The

743 horizontal dot lines in panel B are the mean values of the observed $\delta^{18}O_{TR}$.

744
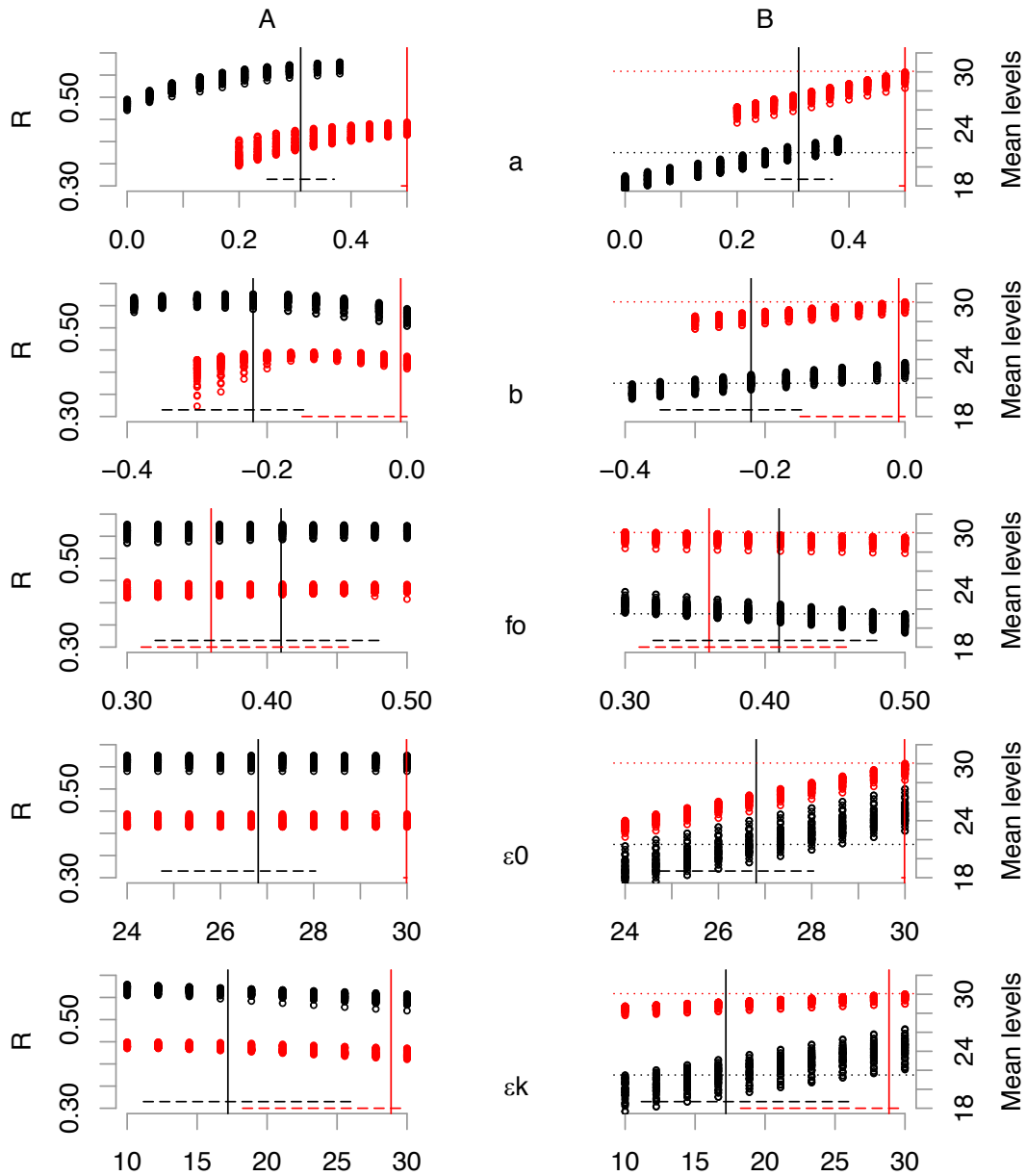
745 **Figure 3** Comparison between observed (red or green) and simulated (grey) $\delta^{18}O_{TR}$ chronologies
746 in Quebec (A and B) and Argentina (C and D), respectively, using GPP (in gC.m^{-2}.day^{-1})
747 simulated by MAIDENiso for each day of the year (DOY) (A and C) or synthetized for
748 maximizing correlations (B and D). The simulations are based on estimated $\delta^{18}O_P$ series. The 50
749 different simulations inferred from the Markov Chain Monte Carlo (MCMC) chains are in dark
750 grey. The ± 1 root mean square error (RMSE) range is represented in light grey. The mean
751 correlation coefficients are significant at 99% level (**).

752
753
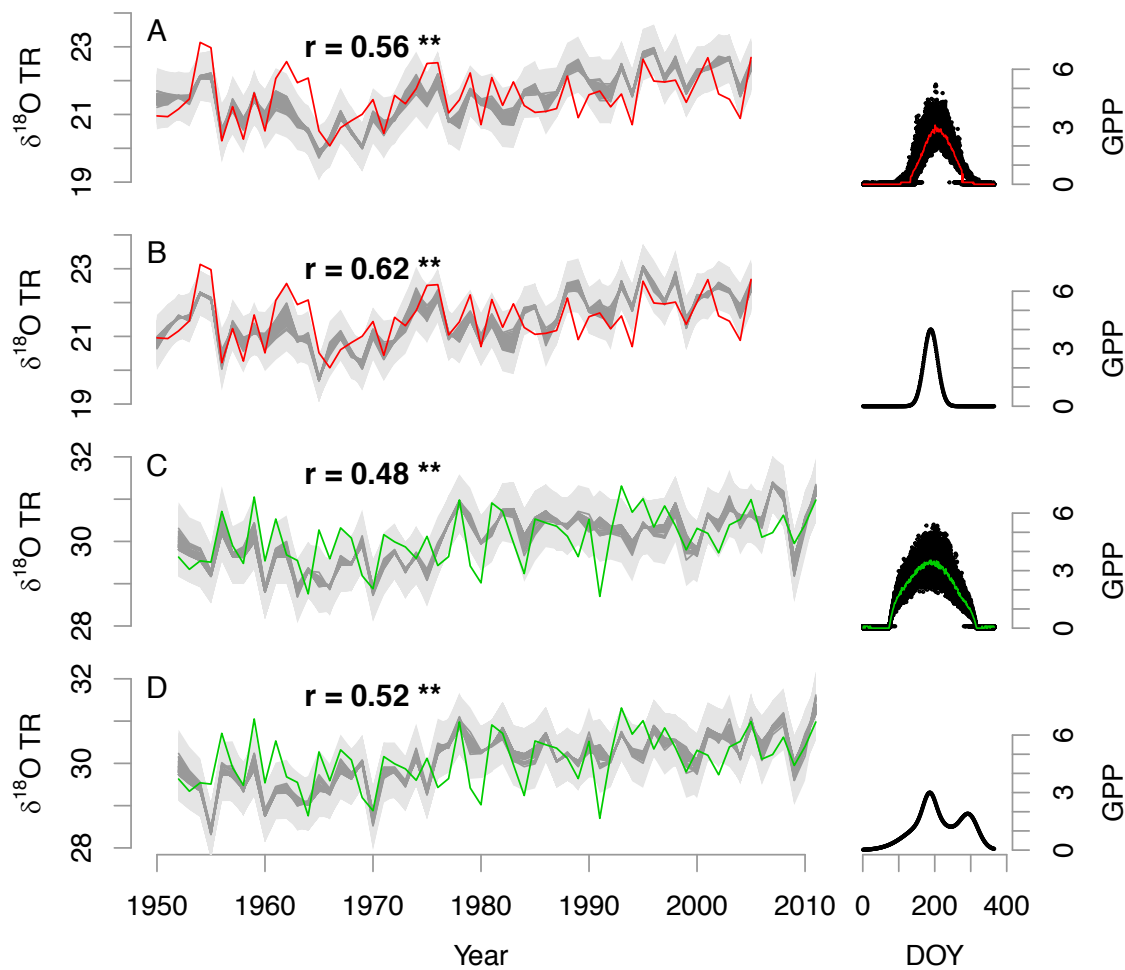
754 **Figure 4** Density distributions of the coefficient of correlation (R) between observed and
755 simulated $\delta^{18}O_{TR}$ chronologies in Quebec and Argentina when the simulations are based on $\delta^{18}O_P$
756 series estimated by the regression model or from the MUGCM and LMDZ-NCEP20 models.
757

758
759
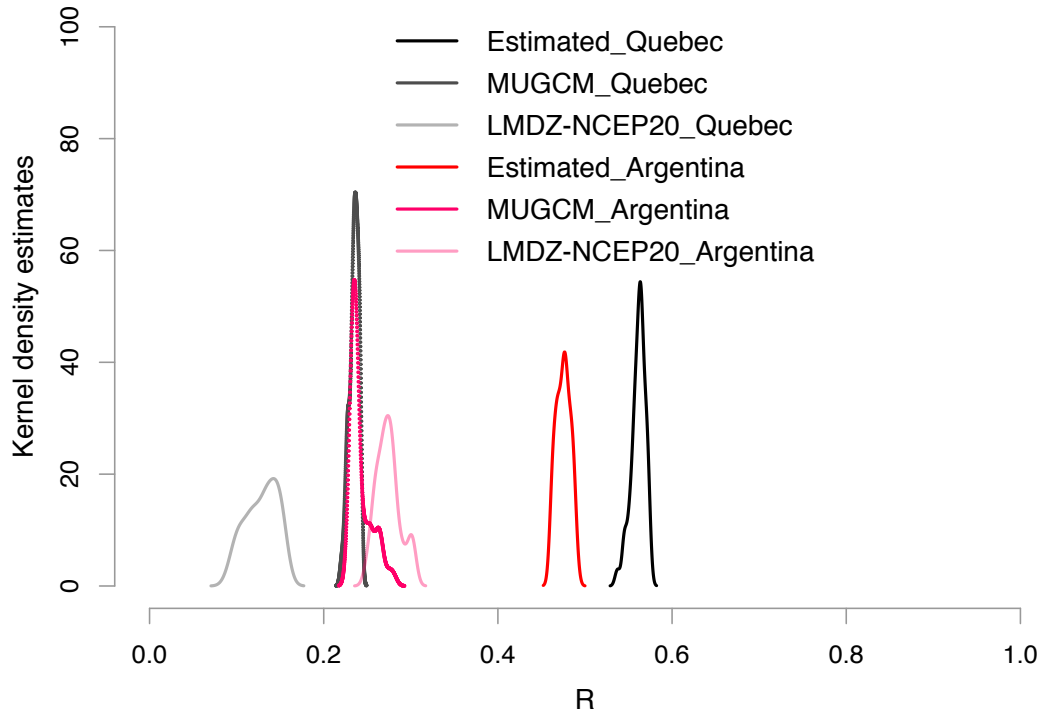
760 **Figure 5** Density distributions of the coefficients of determination (R^2) between the reference
761 simulations and the: 1) XW source experiment simulation ($\delta^{18}O_V$ and h_{air} set as constant, black)
762 and, 2) Leaf water enrichment driven experiment simulation ($\delta^{18}O_{XW}$ set as constant, green) in
763 Quebec (bold line) and Argentina (dashed line).

764

765

766